Performance Evaluation of a High Power, High Energy Density Compact Latent Heat Thermal Energy Store

Mohamed Fadl[1], Philip C. Eames[1*]

[1] *Thermal Energy Storage Group, Centre for Renewable Energy Systems Technology (CREST), Loughborough University, LE11 3TU, UK*
[*]*Corresponding author. Email: p.c.eames@lboro.ac.uk*

ABSTRACT
An experimental study was undertaken to evaluate the thermal performance of a novel compact latent heat thermal energy storage (LH-TES) system. The heat exchanger immersed in the phase change material (PCM) CrodaTherm™ 53, enclosed in a cuboid shaped metal container was a Multi-Plate Heat Exchanger (MPHX). The heat exchanger in the thermal store was comprised of ten individual aluminium rectangular plates mounted vertically spaced at 30 mm intervals. The heat exchanger plates were connected in a parallel flow arrangement with two manifolds used to divide the flow equally between plates. During the charging process, a peak thermal input power of 4.2 kW was measured for an Heat Transfer Fluid (HTF) inlet temperature of 70 °C. To characterize the effect of HTF flow rate on the discharging process, experiments were performed with HTF an inlet temperature of 30 °C with volume flow rates of 2, 3, 4, 5 and 6 L/min. Temperatures within the store at different locations were measured and instantaneous heat output rates and cumulative heat output calculated. Based on the experimental results by adjusting the HTF inlet volume flow rate during the discharging process, the output thermal power and temperature can be controlled for domestic space and water heating applications.

Keywords: *Latent heat storage, Phase change material, Multi-plate heat exchanger, Experimental investigation*

1. INTRODUCTION

Thermal energy storage (TES) is expected to play a significant role in the transition to the wide scale deployment and use of low carbon heating/cooling energy systems. TES is likely to be essential in the electrification of heat in buildings when electricity is produced by mainly low/zero carbon intermittent renewable sources, because it can help to address mismatch between electricity production and heat demand and reduce peaks in electricity demand. The mismatch can be in temperature, time, location or power [1,2]. For example, a combination of TES with Solar Thermal Collectors (STC) increases the possibility of the production and the self-consumption of locally produced renewable energy where the production peak of heat on a daily basis occurs around noon, and Domestic Hot water (DHW) and Space Heating (SH) demand are mostly in the morning and the evening. If different electricity tariffs are available at different times of the day, TES coupled with Air Source Heat Pumps (ASHPs), gives the advantage that it can shift the electricity demands for heat generation (DHW or SH) from peak-load to low-load periods (between 22.00 P.M. and 07.00 A.M.). This can help to balance the grid and reduce electricity bills for homeowners [2,3] by allowing them to shift energy purchases from high-to-low cost periods. Another potential application of TES is in waste heat utilization systems where waste heat availability and utilization periods are different, requiring thermal energy storage to allow heat availability to be shifted in time [4].

P. Droege and L. Quint (eds.), *Proceedings of the International Renewable Energy Storage and Systems Conference (IRES 2023)*, Atlantis Highlights in Engineering 32,
https://doi.org/10.2991/978-94-6463-455-6_14

LH-TES is a particularly attractive technique due to its ability to provides a high energy storage density over a small temperature range, kWh_{th}/m^3, when compared to conventional sensible heat energy storage systems [5]. LH-TES relies on the absorption or release of heat at constant or near constant temperature corresponding to the phase-transition temperature of the specific PCM being used [6]. A major challenge, as reported by many researchers is the low thermal conductivities possessed by many PCMs (usually between 0.2 and 0.7 [W/m K] for organic PCMs) which leads to low rates of heat transfer during charging and discharging [5], which limits the possible application of LH-TES technology in practical systems.

In an attempt to address the issue of low PCM thermal conductivity, there are several different approaches reported in the literature that aim to optimize and improve the thermal performance of LH-TES, including the use of shell and tube (multi-tube) Heat eXchanger, HX [7–11], using a high porosity metal matrix into which the PCM is introduced [12], micro-encapsulation of the PCM [13] or including tubes with different arrangements of fins [14–17]. The general conclusion that can be drawn from the previous studies is that regardless of the PCM used, the thermal performance of a LH-TES can be improved using any of the above listed enhancement techniques, but the effectiveness of each one of them depends on several different factors [18], including the material compatibility of the HX with the PCM being used and the cost of the HX [19].

Increasing the heat transfer area to the PCM is the most simple and efficient method of increasing performance. However, there is always a balance required because, i) increasing the volume fraction of the HX within the store decreases the effective PCM storage volume reducing the quantity of heat that can be stored, ii) extending the length of piping in the HX to improve heat transfer to the PCM store increases the pressure required to pump the HTF through the HX. Approaches such as embedding a graphite matrix in the PCM or augmenting HX pipes with longitudinal/circular fins, can often restrict natural convection in the liquid PCM that increases heat transfer during the phase change processes. Heat transfer enhancement methods generally increase overall cost, add extra weight and decrease heat storage capacity due to the presence of additives [20,21].

To address the mentioned issues, the reported research study evaluates the thermal performance of a low cost LH-TES using a MPHX which can operate with either a STC and/or ASHPs to meet the domestic hot water and/or space heating demand. The evaluated LH-TES configuration achieves high energy storage density, high input/output power without using fins or thermally conductive additives, and it has a large heat transfer surface area compared to a shell and tube HX. The thermal performance was evaluated under different operation conditions during both the charging and discharging processes (HTF inlet/outlet temperature and volume flow rate). The results of a selection of the tests performed in this study are presented in this paper and are expected to be helpful for both benchmarking and model validation data for future numerical studies.

2. EXPERIMENTAL SETUP AND PROCEDURE

2.1. Characterization of the PCM storage material

In this study, a commercial water-insoluble organic PCM CrodaTherm™ 53 with a nominal melting temperature of 53 °C was used for the storage medium [22]. CrodaTherm™ 53 is 100% bio-based and has a phase change transition temperature of around 53 °C. This material was selected because it has a high latent heat capacity (226 kJ/kg), is relatively inexpensive (£5/kg) and has excellent thermophysical stability. The average melting temperature is suitable for heat storage applications with heat provided by an ASHP, flat plate or evacuated tube solar thermal collectors, low-temperature industrial waste heat and to discharge heat at temperatures suitable for domestic hot water (DHW) applications. The detailed thermophysical properties of CrodaTherm™ 53 provided by the manufacturer are listed in Table. 1.

Table. 1. Thermal and physical properties of CrodaTherm™ 53 according to the manufacturer [22].

Property	Typical Value	Units
Peak melting temperature	53	°C
Latent heat, melting	226	kJ/kg
Bio-based content	100	%
Density at 22 °C (solid)	904	kg/m^3
Density at 60 °C (liquid)	829	kg/m^3
Specific heat capacity (solid)	1.9	kJ/(kg·°C)
Specific heat capacity (liquid)	2.2	kJ/(kg·°C)
Volume expansion 22ºC-60 ºC	9.1	%
Thermal conductivity (solid)	0.28	W/(m·°C)
Thermal conductivity (liquid)	0.16	W/(m·°C)

2.2 Experimental test facility

The experimental thermal storage system characterisation was performed using a lab-scale low-temperature thermal store test rig/facility [8,23] at the Centre for Renewable Energy Systems Technology, (CREST), Loughborough University. The lab-scale test rig was designed and built to enable the evaluation of the overall thermal performance of LH-TES during charging and discharging processes under repeatable controlled conditions. A schematic diagram of the test rig is presented in Figure 1. The test rig consists of i) a Heat Transfer Fluid (HTF) cooling circuit, ii) a HTF heating circuit, and iii) the LH-TES under test. Due to the phase change temperature of the PCM and the intended application, water was used as the HTF for both charging and discharging the LH-TES.

The heating loop, which is used to simulate the real heat source during the charging process (i.e. waste heat stream, solar thermal collector, ASHP etc.) consists of a 200 L hot water cylinder in which the HTF is heated to the desired charging temperature using a closed dynamic temperature control system (Peter Huber Kältemaschinenbau, Germany, type: Unistat 510w [24]) with external PT100 sensor probes used to monitor and control the temperature in the tank to the required HTF set point temperature ± 0.1 °C.

The cooling loop contains a 200 L cold water cylinder in which the HTF is cooled down to the desired discharging temperature using a closed dynamic temperature control system (Peter Huber Kältemaschinenbau, Germany, type: Unistat 510w [24]) to simulate the heat demand. The heating/cooling circuits allow the HTF inlet temperature to be set to temperature in the range from 5-95°C.

The heating/cooling loops contain a series of flow control valves and HTF circulation pumps (Pedrollo PQm, 0.37 KW [25]) which are used to circulate and control the direction of the HTF flow between the hot and cold-water tanks and the LH-TES store. A turbine pulse flow rate sensor (Gems™ FT-110 Series, Hall effect [26]) was employed to measure the volume flow rate of the HTF with an accuracy of ± 3% of the reading. The accuracy of the flow rate sensor was confirmed by measuring the time required to fill a 10 L container using different flow rates. Pressure transducers [27] with an accuracy of ±0.25 % of the reading were fitted at the inlet and exit pipes of the LH-TES to measure the pressure drop across the heat exchanger assembly.

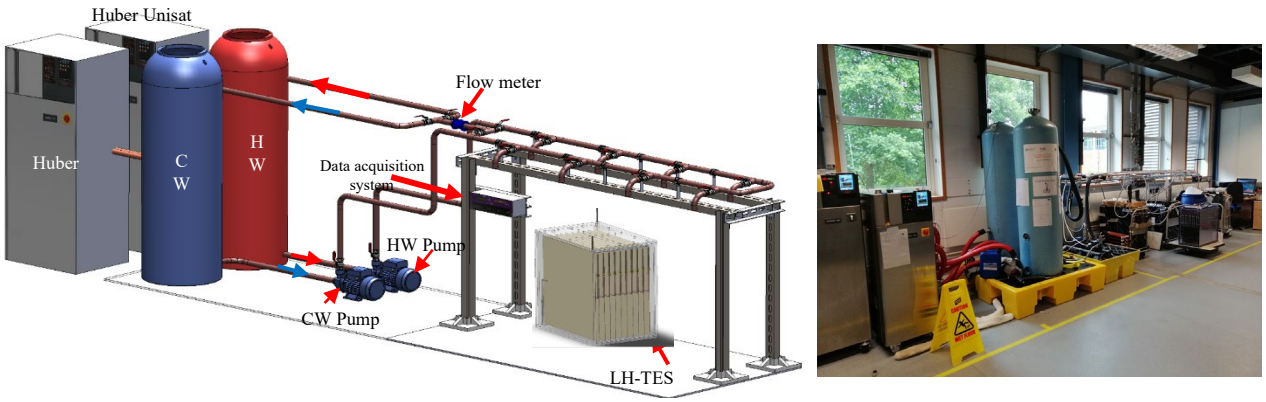

Figure 1 Schematic layout illustrating the experimental thermal store testing facility at Loughborough University and a photograph of the test rig.

3. DESCRIPTION OF THE LHTESS

The novel HX used in this work was based on commercially available aluminium radiant panels [28]. The MPHX was made up of ten panels, mounted vertically, connected in a parallel flow arrangement. Two similar dividing and combining copper manifolds were used to achieve equal flow distribution between the panels for flow in either direction for heating or cooling. Each panel was fabricated from two overlaid layers of aluminium sheeting between which is formed a flow channel through which the HTF circulates. The design of the panel aims to provide good rates of heat exchange, ensure evenly distributed near uniform panel surface temperatures and low HTF flow pressure drops. Each panel has a heat exchange surface area of 0.32 m^2. The spacing between panels in the thermal store was set to 30 mm using spacers.

The storage container was fabricated from 15 mm thick transparent polycarbonate sheet. Transparent store walls were used to allow observation of the melting/solidification process.

The nominal internal dimensions of the container were, height 600 mm, width 350 mm and length 600 mm. The container dimensions allow flexible scaling of the store by adding additional storage modules to meet the thermal energy demands of residential buildings of different sizes. The outer surface of the container was well insulated using 3 cm thick FOAMGLAS® READY BOARD T4^{+} insulation [29] to reduce heat losses from the thermal store to the surroundings during the charging/discharging process.

Images of the radiant panel and the LH-TES are shown in Figures 2 and 3, while Table 2 details the main features of the LH-TES.

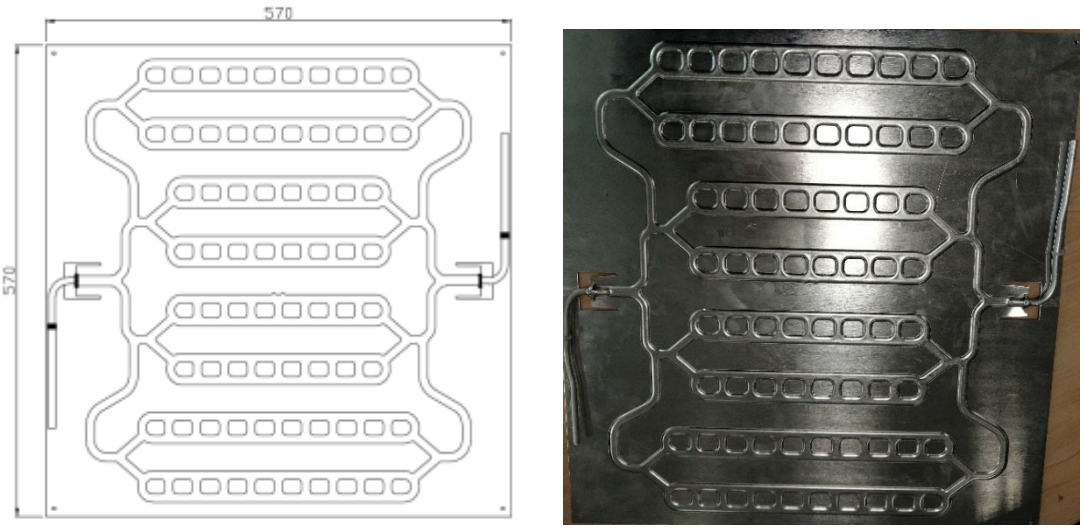

Figure 2 Drawing and image of a heat exchange plate.

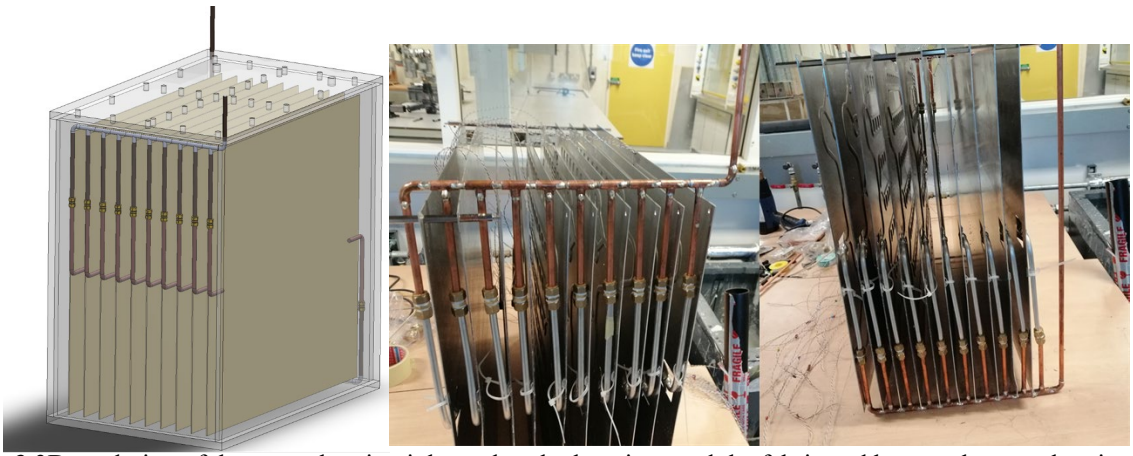

Figure 3 3D rendering of the store showing inlet and outlet locations and the fabricated heat exchanger showing inlet and outlet pipes to each panel to enable equal, parallel flow to each panel.

Table 2. Dimensions and materials used in the LH-TES.

Components	Parameters	Value
Heat exchanger	Material	Aluminium
	Number of the panels	10
Container	Material	Polycarbonate
	Height (mm)	600
	Length (mm)	600
	Width (mm)	350
	Thickness (mm)	15
	Volume of the container (mm^3)	126,000,000
Insulation	Material	FOAMGLAS® READY BOARD T4+
	Thickness (mm)	40
HTF	Material	Water
PCM	Material	CrodaTherm™ 53
	Mass of PCM (kg)	98.0

A total of thirty-four T-type thermocouples were mounted inside the thermal store at the locations indicated in Figure 4 to measure and record the PCM and HX panels surface temperatures prior to filling the store with PCM. Ten of these thermocouples ($T_{Panel(1)}$-$T_{Panel(10)}$) were located on the HX panels at a height of 300mm, (half the store height), to measure and record the panels' temperature response. To obtain sufficient information to understand and interpret the thermal behaviour of the PCM inside the store during charging/discharging, twenty-three thermocouples were mounted in different horizontal and vertical positions between the panels to measure the PCM temperatures as illustrated in Figure 4. The naming nomenclature adopted for these thermocouples, PCM (i, j) enables the location of each thermocouple to be defined. From Figure 4 it can be seen that subscript i, stands for the number of the zone across the heat exchanger in which the thermocouple is located and subscript j, the row/height in the store. Two additional temperature sensors were installed to measure the HTF inlet and outlet temperatures. All the temperature sensors where calibrated and had an accuracy of 0.5 °C. The HTF volume flow rate and temperature sensors were connected to a data logger system linked to a PC enabling data to be measured and recorded on a 5 second basis.

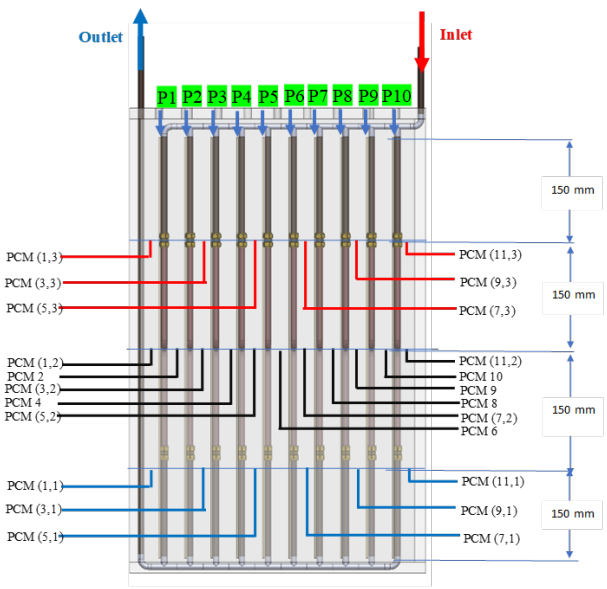

Figure 4 Locations of thermocouples within the store.

4. DATA PROCESSING

4.1 Power and Energy Evaluation

The instantaneous input/output heating power to/from the LH-TES during the charging (melting process) and discharging (solidification process) was calculated utilizing Equation (1).

$$Power_{input/output} = \rho \dot{V} C_{p,water} \Delta T \quad (1)$$

Where ρ and C_p are the density and specific heat capacity of water evaluated at the HTF average temperature, $\dot{V}$ is the volume flow rate of the HTF (m^3/sec), $\Delta T = |T_{inlet} - T_{outlet}|$ is the temperature difference between the inlet and outlet temperature of the HTF (°C).

The total energy input/output at the time of charging/discharging the LH-TES was calculated as the integral of the instantaneous power for the whole duration of the charge/discharge process [30] using Equation (2).

$$Energy_{input/output} = \int_o^t \rho \dot{V} C_p \, \Delta T \, dt \quad (2)$$

4.2 Stored Energy

During the charging/discharging process, the theoretical heat storage capacity of the LH-TES was evaluated by taking account of both sensible heat stored in all components of the store and the latent heat component of the PCM and is expressed by Equation (3). (subscript s for solid and l for liquid)

$$Energy_{storage} = m_{pcm}[C_{p,s}(T_m - T_i) + L_{latent} + C_{p,l}(T_f - T_m)] \quad (3)$$

The average PCM temperature was obtained using Equation (4):

$$T_{PCM\_average} = \frac{\sum_{i=1}^{i=23} T_{PCM}}{9} \quad (4)$$

5. EXPERIMENTAL TESTS

In the charging and discharging tests performed, the initial store state of charge was set before the test commenced. Before the beginning of each charging process, pre-conditioning cold HTF was circulated through the HX in the PCM to achieve an initial PCM temperature of 30 ± 0.5 °C. Concurrently the HTF in the hot circuit was circulated to the hot water store (without flowing through the LH-TES), and heated to and maintained at a specific temperature of either 65 or 70 °C using the dynamic temperature control system. When the hot HTF reached the desired set point inlet

temperature for the charging process, the flow control valves were adjusted to maintain the required flow rate and then the valves directing the hot HTF were set so that the HTF starts to circulate through the LH-TES. The hot HTF was circulated through the LH-TES until the temperatures measured by the thermocouples at the bottom of the store exceeded 60 ˚C. When the LH-TES was fully charged, the low-temperature HTF was circulated through the store and the discharging process commenced, the discharging process was considered finished when the average temperature inside the store reached a specified discharge set point temperature.

The tests were performed for a range of different conditions of HTF inlet temperature and volume flow rate for both charging and discharging experiments, the flow rates and inlet temperatures for the full set of experiments performed are presented in Table 3. with those presented in this paper indicated in bold.

Table 3. Summary of temperatures and flow rates used in the charging and discharging experiments performed.

Mode	PCM initial temperature (°C)	HTF inlet temperature (°C)	HTF volumetric flow rate (L/min)
Charging	**30.0±0.5**	**70.0±0.5**	**2.0**
			4.0
			6.0
		65.0±0.5	2.0
			4.0
			6.0
Discharging	**70.0±0.5**	10.0±0.5	5.0
		20.0±05	5.0
		30.0±0.5	**2.0**
		30.0±0.5	**3.0**
		30.0±0.5	**4.0**
		30.0±0.5	**5.0**
		30.0±0.5	**6.0**
		40.0±0.5	5.0

6. RESULTS AND DISCUSSION

6.1 Repeatability investigation

To establish the repeatability of experiments a series of four charging experiments were performed with a constant HTF inlet temperature of 70 °C and a HTF volume flow rate of 4.0 L/min and the results were compared. Figure 5 shows the transient average temperature of the PCM and the inlet and outlet temperatures of the HTF for the four tests. It is clear from Figure 5 that the average PCM temperature and the HTF inlet and outlet temperatures follow a similar trend with values that are essentially the same for all four experiments.

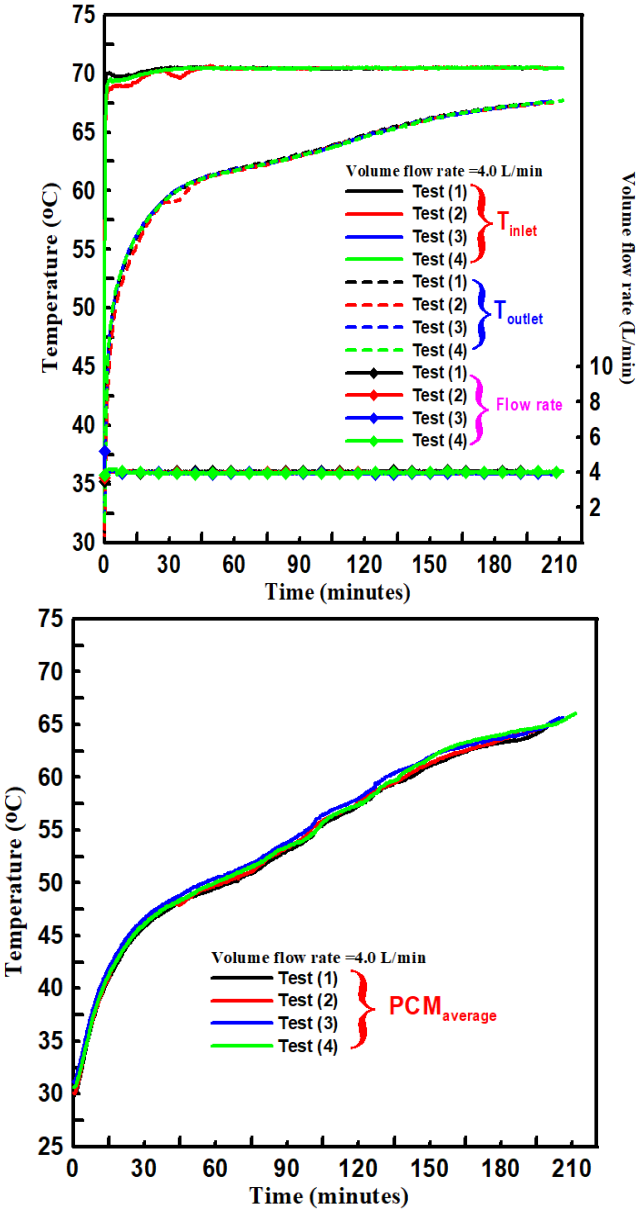

Figure 5 Evaluation of repeatability of experimental tests. Lower graph, average temperature profiles in PCM over time; Upper graph, transient temperature profiles of HTF inlet and outlet temperature and volume flow rate while the system was charging at a set constant inlet temperature of 70 °C and a volume flow rate of 4.0 L/min.

6.2 Multi PHX-LH-TES store charging experiments

The measured PCM temperatures during a charging process in zone (3), between heat exchange panels 2 and 3, at 450, 300 and 150mm from the base of the store and measured at 300mm from the base pf the store on the surfaces of panels 2 and 3 with an inlet HTF

temperature of 70°C and a volume flow of 2 L/min are presented in Figure 6.

It can be seen from Figure 6 that the store charging process can be divided into three stages [31,32]. In the early stages of the charging process, (i.e., up to 45 min) when the PCM is in the solid phase, the heat transfer mechanism to the PCM is dominated by conduction. The temperatures measured by the three thermocouples in the PCM rise rapidly at a similar rate because of the low heat capacity of the solid PCM. The temperatures of the surfaces of panels (2) and (3) in the heat exchanger, show a very fast, near linear increase in temperature (Stage (I)).

Shortly after 45 min, the rate of temperature increase measured on the heat exchanger panels' surfaces decreases when the PCM temperature reaches the melting temperature (around 51°C) and the PCM begins to melt. During the solid-liquid phase transition stage, the temperature of the PCM remains virtually constant due to relatively high latent heat capacity of the PCM. The timing of the transitions varies according to the height within the store, 150, 300, and 450mm (Stage (II)).

As melting progresses, the liquid PCM layer adjacent to the heat exchanger panels' surfaces increases in thickness and natural convection starts to drive the hot liquid PCM upwards due to the density difference between the hotter and colder liquid PCM (buoyancy forces overcome the viscous forces in the liquid PCM). The fluid circulation continues to grow increasing the melt fraction and the temperature of the heat exchanger panels increase slowly. The temperature measured at a height of 450mm in zone (3) are higher than those measured at 150 and 300mm and natural convection is the dominant mode of heat transfer from the hot surfaces of the panels to the PCM (Stage (III)). Finally, the PCM temperature reaches a steady-state temperature close to the heat exchanger panels temperature.

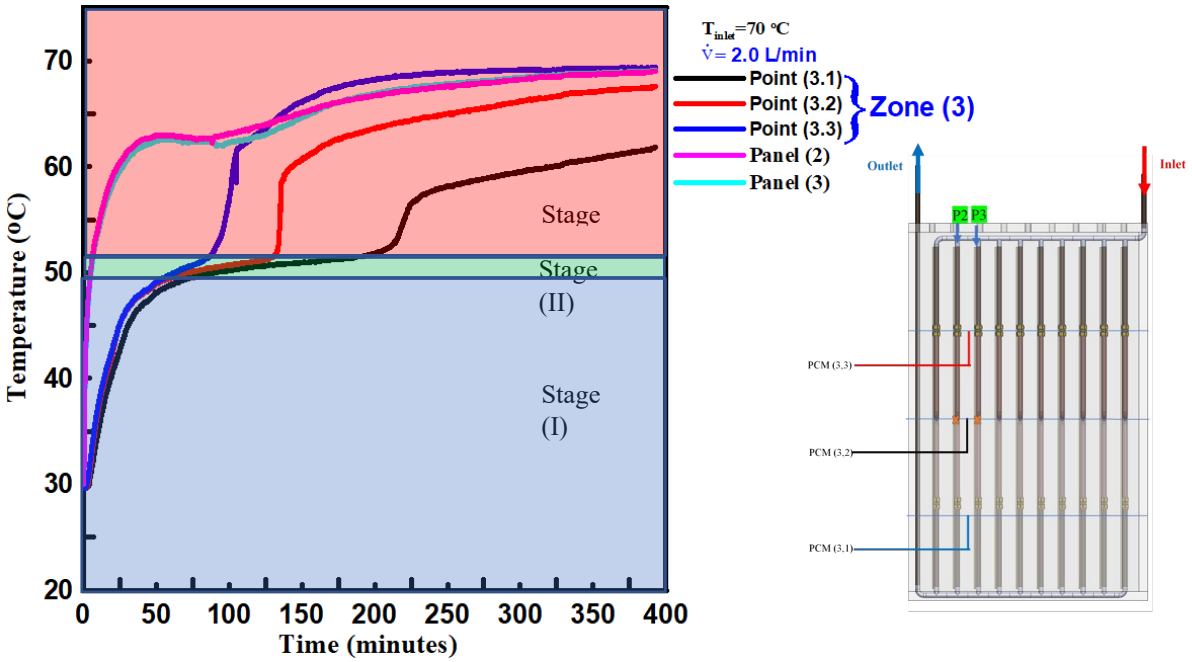

Figure 6 PCM temperature profiles during charging process in zone (3) at 150, 300 and 450mm from the base of the store and the temperatures of heat exchange panels (2) and (3) measured at a height of 300mm.

6.3 Effect of hot HTF volume flow rate on charging time

The effect of HTF volume flow rate on the thermal performance of the LH-TES was examined using three HTF volume flow rates: 2.0, 4.0 and 6.0 L/min and a HTF inlet temperature set to 70 °C during the charging process.

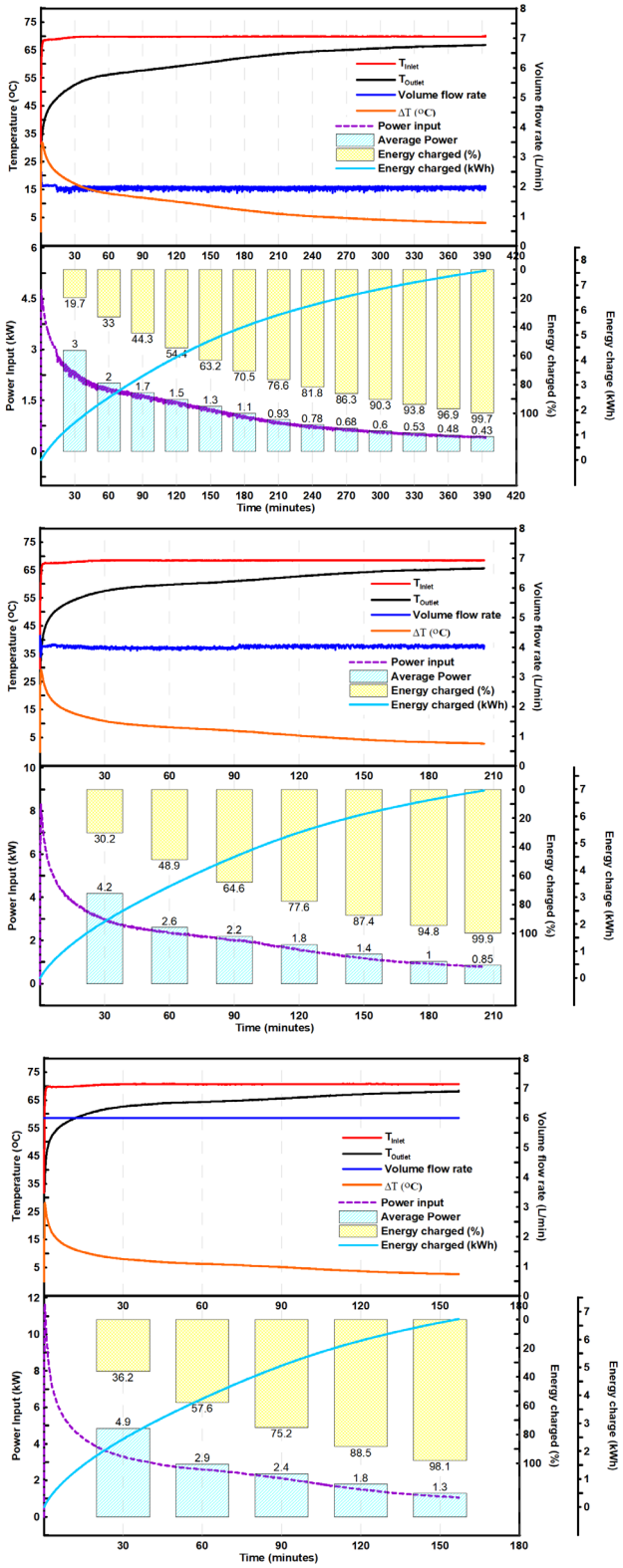

Figure 7 HTF inlet/outlet temperature, instantaneous/average thermal power and heat charged during the charging process for 2.0, 4.0, 6.0 L/min flow rates.

Figure 7 shows the transient HTF inlet/outlet temperatures, HTF inlet-outlet temperature difference, cumulative energy-input, transient and average power input for the 3 HTF volume flow rates. As can be seen in Figure 7 the amount of energy stored in the LH-TES was approximately 7.2 ±0.4 kWh. The general trend is that the amount of energy transferred to the LH-TES (power input) quickly dropped in the first 30 minutes, then subsequently decreased nearly linearly until the end of the charging process. This is a consequence of the decreasing temperature difference between the HTF and the melting/liquid PCM. As the PCM temperature increases, the temperature difference between the HX panel surface and the PCM decreases. The driving force for heat transfer into the store, the temperature difference is largest when the charging process begins [38].

From Figure 7 the impact of changing HTF volume flow rate for constant HTF inlet temperature on input power can be seen and is more pronounced during the initial stage of the charging process. The average input power rate at a volume flow rate of 2.0 L/min in the first 30 minutes was 3.0 kW, increasing to 4.0 kW and 4.9 kW when the HTF volume flow rate increased to 4.0 L/min and 6.0 L/min, respectively. It can also be seen that the HTF outlet temperature rises rapidly during the first 30 minutes of charging, during the sensible heat storage phase and then slowly increases towards the HTF inlet temperature.

After 120 minutes from the charging process commencing, for a flow rate 6.0 L/min, the total amount of thermal energy stored in the form of sensible and latent heat (Stage(I) and Stage (II)) in the LH-TES was about 88.5 % of the total amount of thermal energy stored during the full experiment. This means that the sensible heat stored in the liquid PCM during Stage (III) is relatively small, and that the charging process could be stopped with only a small reduction in total heat stored after Stage (II) to reduce the charging time.

6.4 Effect of cold HTF volume flow rate on discharging time

A parametric investigation to determine the influence of the HTF volume flow rate on the thermal performance of the LH-TES during the discharging process was conducted by varying the HTF volume flow rate. Discharging experiments were performed at five HTF volume flow rates of 2.0, 3.0, 4.0, 5.0 and 6.0 L/min with a constant HTF inlet temperature of 30 ±0.5 °C.

Figure 8 presents the HTF inlet and outlet temperatures, HTF inlet-outlet temperature difference, average and instantaneous power output and cumulative energy discharged for discharging experiments using HTF volume flow rates of 2.0, 4.0 and 6.0 L/min. From figure 8 it can be seen that the HTF volume flow rate has a significant impact on the discharging rate and heat transfer to the HTF. Due to the high temperature difference between the store and the HTF at the start of the discharging process, the rate of cumulative thermal energy extraction from the store by the HTF is high, which leads to the temperature difference driving heat transfer being reduced.

The experimental results show that the effect of HTF volume flow rate on discharge power is significant. For the tests performed, the higher the HTF volume flow rate, the higher the instantaneous and average power output measured during the tests. In the first 30 minutes, the maximum and minimum average output powers were 5.26 kW and 3.17 kW for HTF volume flow rates of 6.0 L/min and 2.0 L/min, respectively.

It can be seen that after 90 minutes of the discharging process, the cumulative thermal energy discharged to the HTF was 3.69 kWh, 4.69 kWh, and 5.2 kWh for HTF volume flow rates of 2.0, 4.0 and 6.0 L/min, respectively.

7. CONCLUSIONS

In this paper, an experimental investigation of the thermal performance of a novel compact LH-TES prototype using a multi-plate heat exchanger is reported. The prototype system was evaluated under controlled conditions for both the charging (melting) and discharging (solidification) processes. A detailed parametric study examined the effects of varying the HTF volume flow rate on charging and discharging. The following observations from the experimental study can be made:

Natural convection plays an important role during the charging process, it does not play a major role during the discharging process.

During the initial periods of the charging process, heat transfer is conduction-dominated.

During the charging process, at HTF inlet temperature of 70ºC, increasing the HTF flow rate from 2.0 L/min to 4.0 L/min and 6.0 L/min decreases the charging time by 41% and 60% respectively.

The total amount of energy stored in the multi PHX-LH-TES store was 7.2 ±0.4 kWh during the charging process for HTF inlet temperature of 70ºC.

During the initial stage of the charging process with a HTF inlet temperature of 70ºC, the average input power rate at a volume flow rate of 2.0 L/min in 30 minutes

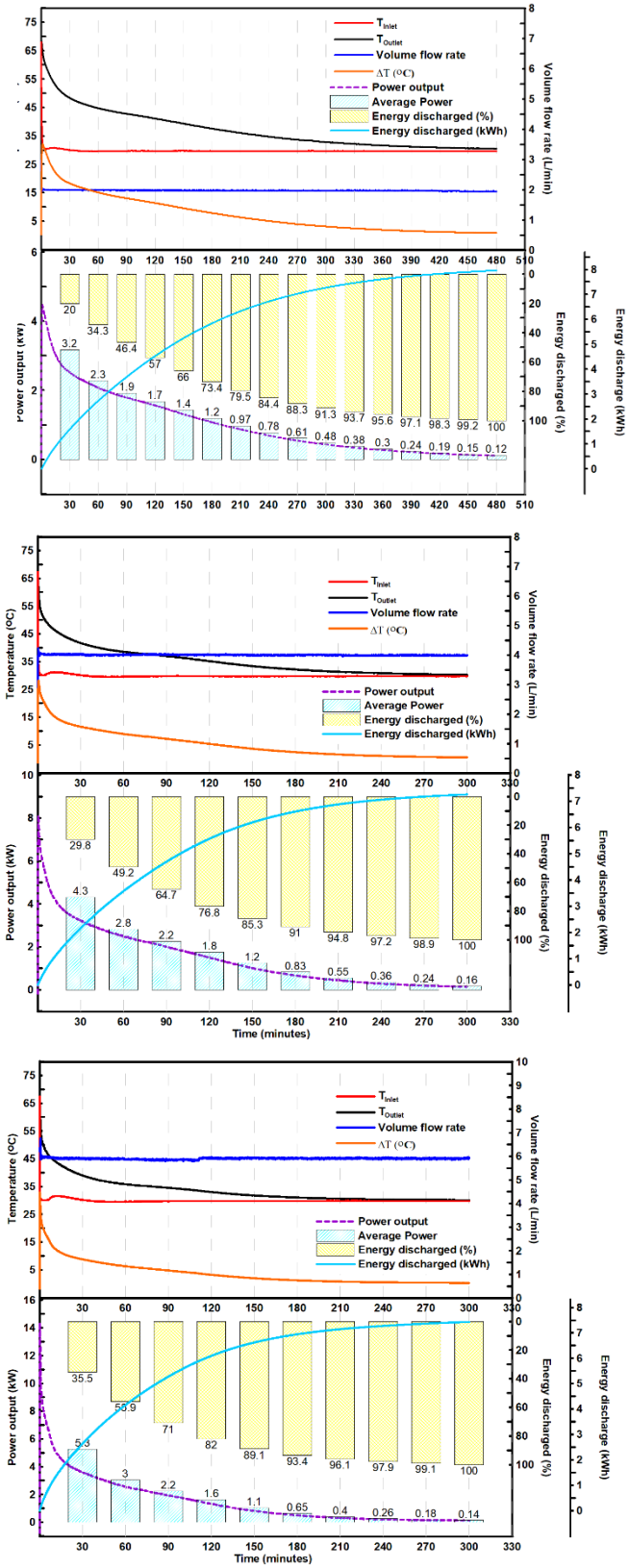

Figure 8 HTF inlet and outlet temperature, instantaneous and average thermal power, and energy discharge rate for HTF volume flow rates of 2.0, 4.0 and 6.0 L/min.

was 3.0 kW, which increased to 4.0 kW and 4.9 kW when the HTF volume flow rate increased from 4.0 L/min to 6.0 L/min, respectively.

In the first 30 minutes of discharging with an HTF inlet temperature of 30°C the maximum and minimum average output powers were 5.26 kW and 3.17 kW for HTF volume flow rates of 6.0 L/min and 2.0 L/min, respectively.

After 90 minutes of the discharging process with a HTF inlet temperature of 30°C the cumulative thermal energy discharged to the HTF was 3.69 kWh, 4.69 kWh, and 5.2 kWh for HTF volume flow rates of 2.0, 4.0 and 6.0 l/min, respectively.

AUTHORS' CONTRIBUTIONS

M Fadl: Conceptualization, Experimental Methodology and Testing, Data Analysis, Writing – original draft. PC Eames: Conceptualization, Experimental Methodology, Data Analysis, Writing - review & editing, Supervision, Funding acquisition.

ACKNOWLEDGEMENT

The support of the EPSRC through The Active Building Centre (ABC) project which received funding from the Engineering and Physical Sciences Research Council (EPSRC) grant EP/S016627/1 and the LoT-NET program grant EP/R045496/1 are gratefully acknowledged.

REFERENCES

[1] Ibrahim NI, Al-Sulaiman FA, Rahman S, Yilbas BS, Sahin AZ. Heat transfer enhancement of phase change materials for thermal energy storage applications: A critical review. Renew Sustain Energy Rev 2017;74:26–50. https://doi.org/10.1016/j.rser.2017.01.169.

[2] Eames P, Dennis L, Victoria H, Romanos P. The Future Role of Thermal Energy Storage in the UK Energy System: An assessment of the Technical Feasibility and Factors Influencing Adoption. Res Rep (UKERC London) 2014:56. https://doi.org/10.1016/j.injury.2007.11.414.

[3] Le KX, Huang MJ, Shah N, Wilson C, Artain P Mac, Byrne R, et al. High temperature air source heat pump coupled with thermal energy storage: Comparative performances and retrofit analysis. Energy Procedia, vol. 158, Elsevier Ltd; 2019, p. 3878–85. https://doi.org/10.1016/j.egypro.2019.01.857.

[4] Farid MM, Khudhair AM, Razack SAK, Al-Hallaj S. A review on phase change energy storage: materials and applications. Energy Convers Manag 2004;45:1597–615. https://doi.org/10.1016/j.enconman.2003.09.015.

[5] Agyenim F, Hewitt N, Eames P, Smyth M. A review of materials, heat transfer and phase change problem formulation for latent heat thermal energy storage systems (LHTESS). Renew Sustain Energy Rev 2010;14:615–28. https://doi.org/10.1016/j.rser.2009.10.015.

[6] Ning-Wei Chiu J. Latent heat thermal energy storage for indoor comfort control. 2013.

[7] Shen G, Wang X, Chan A. Experimental investigation of heat transfer characteristics in a vertical multi-tube latent heat thermal energy storage system. Energy Procedia 2019;160:332–9. https://doi.org/10.1016/j.egypro.2019.02.165.

[8] Fadl M, Eames PC. An experimental investigation of the heat transfer and energy storage characteristics of a compact latent heat thermal energy storage system for domestic hot water applications. Energy 2019;188:116083. https://doi.org/10.1016/j.energy.2019.116083.

[9] Joybari MM, Seddegh S, Wang X, Haghighat F. Experimental investigation of multiple tube heat transfer enhancement in a vertical cylindrical latent heat thermal energy storage system. Renew Energy 2019;140:234–44. https://doi.org/10.1016/j.renene.2019.03.037.

[10] Egea A, Solano JP, Pérez-García J, García A. Solar-driven melting dynamics in a shell and tube thermal energy store: An experimental analysis. Renew Energy 2020;154:1044–52. https://doi.org/10.1016/j.renene.2020.03.078.

[11] Fadl MS, Eames PC. An experimental investigation of the heat transfer and energy storage characteristics of a latent heat thermal energy storage system with a vertically-oriented multi-pass tube heat exchanger for domestic hot water applications. Eurotherm Semin #112 Adv Therm Energy Storage 2019.

[12] Kumar A, Saha SK. Experimental and numerical study of latent heat thermal energy storage with high porosity metal matrix under intermittent heat loads. Appl Energy 2020;263:114649. https://doi.org/10.1016/j.apenergy.2020.114649.

[13] Sakai H, Sheng N, Kurniawan A, Akiyama T, Nomura T. Fabrication of heat storage pellets composed of microencapsulated phase change material for high-temperature applications. Appl Energy 2020;265:114673. https://doi.org/10.1016/j.apenergy.2020.114673.

[14] Hosseinzadeh K, Moghaddam MAE, Asadi A, Mogharrebi AR, Ganji DD. Effect of internal fins along with Hybrid Nano-Particles on solid process in star shape triplex Latent Heat Thermal Energy Storage System by numerical simulation. Renew Energy 2020;154:497–507. https://doi.org/10.1016/j.renene.2020.03.054.

[15] Pu L, Zhang S, Xu L, Li Y. Thermal performance optimization and evaluation of a radial finned shell-and-tube latent heat thermal energy storage unit. Appl Therm Eng 2020;166:114753. https://doi.org/10.1016/j.applthermaleng.2019.114753.

[16] Karami R, Kamkari B. Experimental investigation of the effect of perforated fins on thermal performance enhancement of vertical shell and tube latent heat energy storage systems. Energy Convers Manag 2020;210:112679. https://doi.org/10.1016/j.enconman.2020.112679.

[17] Deng S, Nie C, Wei G, Ye WB. Improving the melting performance of a horizontal shell-tube latent-heat thermal energy storage unit using local enhanced finned tube. Energy Build 2019;183:161–73. https://doi.org/10.1016/j.enbuild.2018.11.018.

[18] Naghavi MS, Ong KS, Mehrali M, Badruddin IA, Metselaar HSC. A state-of-the-art review on hybrid heat pipe latent heat storage systems. Energy Convers Manag 2015;105:1178–204. https://doi.org/10.1016/j.enconman.2015.08.044.

[19] Seddegh S, Wang X, Henderson AD, Xing Z. Solar domestic hot water systems using latent heat energy storage medium: A review. Renew Sustain Energy Rev 2015;49:517–33. https://doi.org/10.1016/j.rser.2015.04.147.

[20] Youssef W, Ge YT, Tassou SA. CFD modelling development and experimental validation of a phase change material (PCM) heat exchanger with spiral-wired tubes. Energy Convers Manag 2018;157:498–510. https://doi.org/10.1016/j.enconman.2017.12.036.

[21] Zhang C, Yu M, Fan Y, Zhang X, Zhao Y, Qiu L. Numerical study on heat transfer enhancement of PCM using three combined methods based on heat pipe. Energy 2020;195:116809. https://doi.org/10.1016/j.energy.2019.116809.

[22] croda. CrodaTherm 53, Croda Phase Change Materials 2018. https://www.crodatherm.com (accessed December 9, 2019).

[23] Fadl M, Eames P. Thermal Performance Analysis of the Charging/Discharging Process of a Shell and Horizontally Oriented Multi-Tube Latent Heat Storage System. Energies 2020;13:6193. https://doi.org/10.3390/en13236193.

[24] Huber Unistat 510w 2019. https://www.huber-online.com/us/product_datasheet.aspx?no=1005.0061.01 (accessed December 14, 2018).

[25] Pumps with peripheral impeller n.d. https://www.pedrollo.com/en/pq-pumps-with-peripheral-impeller/127 (accessed December 14, 2018).

[26] Flow Switch Gems Sensors FS-3 | RS Components n.d. https://uk.rs-online.com/web/p/flow-switches/3956940/ (accessed July 12, 2019).

[27] RS PRO for Air, Gas, Hydraulic Fluid, Liquid, Water Gauge n.d. https://uk.rs-online.com (accessed April 29, 2020).

[28] ahhm-radiant.com n.d. https://ahhm-radiant.com/wp-content/uploads/2018/05/Ahhm-Manual_FINAL.pdf (accessed December 9, 2019).

[29] www.foamglas.com. Foamglas 2020:1–2. https://www.foamglas.com/en-gb/products/fgbt4slabs (accessed December 9, 2019).

[30] Palomba V, Brancato V, Frazzica A. Thermal performance of a latent thermal energy storage for exploitation of renewables and waste heat: An experimental investigation based on an asymmetric plate heat exchanger. Energy Convers Manag 2019;200:112121. https://doi.org/10.1016/j.enconman.2019.112121.

[31] Fadl M, Eames PC. A comparative study of the effect of varying wall heat flux on melting characteristics of phase change material RT44HC in rectangular test cells. Int J Heat Mass Transf 2019;141:731–47.

[32] Fadl M, Eames PC. An experimental investigations of the melting of RT44HC inside a horizontal rectangular test cell subject to uniform wall heat flux. Int J Heat Mass Transf 2019;140:731–42. https://doi.org/10.1016/j.ijheatmasstransfer.2019.06.047.